Supporting Information

Effects of Multiple-Bond Ruptures in Force Spectroscopy Measurements of Interactions between Fullerene C_{60} Molecules in Water

Chao Gu, Andrea Kirkpatrick, Chad Ray, Senli Guo and Boris B. Akhremitchev*

Department of Chemistry, Duke University, Durham, NC 27708

1. Derivation of the probability density for the two-bond rupture force

Rupture of two parallel bonds is schematically illustrated in Figure S1. Since either of two bonds might rupture and be detected as one rupture event, the survival probability of two bonds equals to the product of two survival probabilities:

$$S(F_\Sigma) = S_1(F_\Sigma) \cdot S_2(F_\Sigma) \quad \text{(S1)}$$

Here $F_\Sigma = F_1 + F_2$ and S is the bond survival probability. The probability density function (PDF) $P(F)$ can be calculated according to:

$$P(F_\Sigma) = \frac{dS(F_\Sigma)}{dF_\Sigma} = S_1(F_\Sigma) \cdot P_2(F_\Sigma) + S_2(F_\Sigma) \cdot P_1(F_\Sigma) \quad \text{(S2)}$$

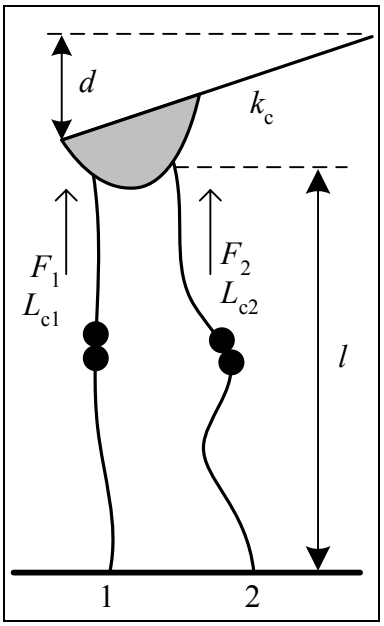

Figure S1. Rupture of two parallel bonds

In AFM experiments with the probe moving at constant velocity v the survival probability of a single bond will differ from the survival probability when two bonds are in parallel due to the different dynamics of loading. As shown in the paper this difference is small and it will not be considered below. Therefore, the PDF becomes:

$$P(F_\Sigma) = s(F_1) \cdot p(F_2) \cdot \frac{dF_2}{dF_\Sigma} + s(F_2) \cdot p(F_1) \cdot \frac{dF_1}{dF_\Sigma} \quad \text{(S3)}$$

Here F_1 and F_2 are the forces along the shorter and the longer tether, respectively and the small letters denote the functions of the individual bonds. By using the asymptotic freely jointed chain

* boris.a@duke.edu

(aFJC) model[1] (in the high force limit), the forces along individual tethers can be related to the total force $F_\Sigma = F_1 + F_2$ according to:

$$F_1 = \frac{F_\Sigma \delta L_c - F_K(2+\delta L_c) + \sqrt{4F_K F_\Sigma \delta L_c + (F_\Sigma \delta L_c - F_K(2+\delta L_c))^2}}{2\delta L_c} \qquad (S4)$$
$$F_2 = F_\Sigma - F_1$$

Here δL_c is the relative difference in the length between the longer and the shorter tether $\delta L_c = \left(L_{c,2} - L_{c,1}\right)/L_{c,1}$ and F_K is the characteristic thermal Kuhn force $F_K = k_B T/a$ where k_B is the Boltzmann's constant, T is the absolute temperature and a is the Kuhn length.

The relative difference between the tether lengths δL_c is not controlled in the experiments. Therefore, in order to obtain PDF to fit the experimental histograms the distribution given by Eq S3 should be averaged over the distribution of δL_c values:

$$\Pi(F_\Sigma) = \frac{\int_0^{\delta L_c^{\max}} p_t(\delta L_c)\cdot P(F_\Sigma, \delta L_c)\, d\delta L_c}{\int_0^{\delta L_c^{\max}} p_t(\delta L_c)\, d\delta L_c} = \frac{\int_0^{\delta L_c^{\max}} P(F_\Sigma, \delta L_c)\, d\delta L_c}{\delta L_c^{\max}} \qquad (S5)$$

Here $p_t(\delta L_c)$ is the probability of encounter a particular value of δL_c. In the second equality of the above equation it is assumed that this probability is constant. Substituting Eq S3 into Eq S5 and approximating $dF_1/dF_\Sigma = dF_2/dF_\Sigma = 1/2$, the averaged PDF becomes

$$\Pi(F_\Sigma) = \frac{\int_0^{\delta L_c^{\max}} \left\{s(F_1)\cdot p(F_2) + s(F_2)\cdot p(F_1)\right\} d\delta L_c}{2\delta L_c^{\max}}$$
$$\simeq \frac{s\left(F_1, \delta L_c^{\max}/2\right)\int_0^{\delta L_c^{\max}} p(F_2)\, d\delta L_c + s\left(F_2, \delta L_c^{\max}/2\right)\int_0^{\delta L_c^{\max}} p(F_1)\, d\delta L_c}{2\delta L_c^{\max}} \qquad (S6)$$

Integrals in Eq S6 can be calculated approximately by using the linearized Eq S4 for small values of δL_c :

$$F_1 = \frac{F_\Sigma}{2} + \delta L_c \frac{F_\Sigma\left(F_\Sigma - 2F_K\right)}{8F_k}$$
$$F_2 = \frac{F_\Sigma}{2} - \delta L_c \frac{F_\Sigma\left(F_\Sigma - 2F_K\right)}{8F_K} \qquad (S7)$$

Using Eqs S7 to change the integration variable to force in Eq S6 and approximating the survival probability under the integral by a constant value computed in the middle of the interval, Eq S6 becomes

$$\Pi(F_\Sigma) \simeq \frac{4F_K}{F_\Sigma(F_\Sigma - 2F_K)\delta L_c^{\max}} \times \left\{ s\left(F_1, \delta L_c^{\max}/2\right) \int_{\frac{F_\Sigma}{2} - \delta L_c^{\max}}^{\frac{F_\Sigma}{2}} \frac{F_\Sigma(F_\Sigma - 2F_K)}{8F_K} p(F_2)\, dF_2 + s\left(F_2, \delta L_c^{\max}/2\right) \int_{\frac{F_\Sigma}{2}}^{\frac{F_\Sigma}{2} + \delta L_c^{\max}} \frac{F_\Sigma(F_\Sigma - 2F_K)}{8F_K} p(F_1)\, dF_1 \right\} \quad \text{(S8)}$$

Computing the integrals in Eq S8 gives

$$\Pi(F_\Sigma) \simeq \frac{4F_K}{F_\Sigma(F_\Sigma - 2F_K)\delta L_c^{\max}} \times \left\{ s\left(\frac{F_\Sigma}{2} + \delta L_c^{\max} \frac{F_\Sigma(F_\Sigma - 2F_K)}{16F_K}\right)\left[s\left(\frac{F_\Sigma}{2} - \delta L_c^{\max} \frac{F_\Sigma(F_\Sigma - 2F_K)}{8F_K}\right) - s\left(\frac{F_\Sigma}{2}\right)\right] + s\left(\frac{F_\Sigma}{2} - \delta L_c^{\max} \frac{F_\Sigma(F_\Sigma - 2F_K)}{16F_K}\right)\left[s\left(\frac{F_\Sigma}{2}\right) - s\left(\frac{F_\Sigma}{2} + \delta L_c^{\max} \frac{F_\Sigma(F_\Sigma - 2F_K)}{8F_K}\right)\right]\right\} \quad \text{(S9)}$$

For small values of δL_c Eq S9 can be further simplified as

$$\Pi(F_\Sigma) \simeq \frac{4F_K}{F_\Sigma(F_\Sigma - 2F_K)\delta L_c^{\max}} s\left(\frac{F_\Sigma}{2}\right) \times \left[s\left(\frac{F_\Sigma}{2} - \delta L_c^{\max} \frac{F_\Sigma(F_\Sigma - 2F_K)}{16F_K}\right) - s\left(\frac{F_\Sigma}{2} + \delta L_c^{\max} \frac{F_\Sigma(F_\Sigma - 2F_K)}{16F_K}\right)\right] \quad \text{(S10)}$$

Numerical calculations show that Eq S10 approximates the total PDF accurately only for very small δL_c (<0.02). The inaccuracy of this approximation stems from the approximate nature of linearization used in Eqs S7. Therefore for larger $\delta L_c^{\max}$ values the approximate total PDF can be more accurately calculated without using this linearization. Therefore, using Eqs S7 the approximate PDF becomes

$$\Pi(F_\Sigma) \simeq s\left(\frac{F_\Sigma}{2}\right) \cdot \left[s(F_2) - s(F_1)\right] / (F_1 - F_2) \quad \text{(S11)}$$

Here forces F_1 and F_2 are calculated according to Eqs S4 by substituting $\delta L_c^{\max}$ in place of δL_c.

Approximation $dF_1/dF_\Sigma = dF_2/dF_\Sigma = 1/2$ that was used above (equation S6) spoils the normalization of PDF calculated according to Eq S11 when $\delta L_c^{\max} > 0.02$ and forces along individual tethers become sufficiently different. The normalization is improved when Eq S11 is multiplied by a constant factor that depends on $\delta L_c^{\max}$:

$$\Pi(F_\Sigma) \simeq \left(1 + 2\,\delta L_c^{\max}\right) \cdot s\left(\frac{F_\Sigma}{2}\right) \cdot \left[s(F_2) - s(F_1)\right] / (F_1 - F_2) \qquad \text{(S12)}$$

This equation is Eq 7 in the manuscript.

2. Extended freely jointed chain model

This model is an extension of the commonly used freely jointed chain (FJC) model. FJC model predicts extension of the polymer chain $x(F)$ with the Kuhn length a and contour length L_c as a function of applied force F according to

$$x(F) = L_c \cdot \left[\coth\left(F \cdot a / k_B \cdot T \right) - k_B \cdot T / F \cdot a \right] \qquad \text{(S13)}$$

where k_B is the Boltzmann's constant and T is the temperature. This equation is often written as $x(\beta) = L_c \cdot \mathcal{L}(\beta)$ were $\mathcal{L}(x)$ is the Langevin function and $\beta = F \cdot a/(k_B \cdot T)$.

Besides an entropic elasticity of the polymer chain included in the FJC model, the extended model includes elongation of the PEG chain due to monomer elasticity as well as conformational transition between helical and planar conformations of the PEG chain in aqueous solutions.[2] In this model, the contour length of a stretched PEG polymer consists of the lengths of polymer segments at two different conformations, planar and helical:

$$L_c = N_{planar} \cdot L_{planar} + N_{helical} \cdot L_{helical} \qquad \text{(S14)}$$

Here N_{planar} and $N_{helical}$ are the numbers of segments in planar and helical conformations respectively. L_{planar} and $L_{helical}$ are the corresponding monomer lengths that are fixed to 3.58 Å and 2.8 Å respectively in our calculations.[2] Contour length defined by Eq S14 can be related to common definition of contour length (the maximum distance between ends of the linear polymer chain) by noting that if $N_{helical}$ and N_{planar} have fixed (force-independent) values then usual definition of contour length can be applied. The ratio of $N_{helical}$ to N_{planar} depends on the applied force according to

$$\frac{N_{helical}}{N_{planar}} = e^{\Delta G(F)/k_B \cdot T}$$
$$\Delta G(F) = \Delta G_0 - F \cdot \left(L_{planar} - L_{helical} \right) \quad \text{(S15)}$$

Here $\Delta G(F)$ is the force-dependent free energy difference between the two states and ΔG_0 is this difference at zero applied load that is fixed to 7.48 kJ/mol in our calculations.[2] The overall extension of the PEG chain with N monomers is:

$$x(F) = N \cdot \left(\frac{L_{planar}}{e^{+\Delta G/k_B \cdot T} + 1} + \frac{L_{helical}}{e^{-\Delta G/k_B \cdot T} + 1} \right) \cdot \left[\coth(\beta) - 1/\beta \right] + N \cdot \frac{F}{K_S} \quad \text{(S16)}$$

Here the segmental elasticity K_S provides the chain extension at high loads and was established to be equal to 150 N/m. [2] Because of the relatively small number of segments in the PEG chains that were used in experiments (~80) and relatively low rupture forces (~100 pN), the last term contributes only ~0.05 nm to the extension at the maximum load and therefore this term was omitted in our data analysis. Eq S16 can be re-written to include the contour length defined as the product of the planar segment length and the number of monomers:

$$x(F) = L_{c,\max} \cdot \left(\frac{1}{e^{+\Delta G(F)/k_B \cdot T} + 1} + \frac{L_{helical}}{L_{planar}} \frac{1}{e^{-\Delta G(F)/k_B \cdot T} + 1} \right) \cdot \left[\coth(\beta) - 1/\beta \right] \quad \text{(S17)}$$

This model was used to fit the force curves with two free parameters: the maximum contour length $L_{c,max}$ and the Kuhn length. The Kuhn length was allowed to vary to obtain a close fit to the data near the rupture point.

In AFM experiments with constant probe velocity the time-dependent position of the base of the cantilever z is the sum of the tether deflection and the polymer stretching. Therefore

$$z = v \cdot t = \frac{F}{k_c} + x(F) \quad \text{(S18)}$$

Here v is the probe velocity, t is the time, and k_c is the cantilever spring constant. Therefore, the instantaneous loading rate v_F used in Eq 1 of the manuscript is

$$v_F = \frac{dF}{dt} = \frac{v \cdot k_c}{1 + x'(F)} \quad \text{(S19)}$$

where $x'(F)$ in the denominator is the derivative of the PEG tether extension (Eq S17) with respect to force. This is an analytical function that can be used directly in calculations of the probability density. Similarly, when using the standard FJC model the loading rate can be obtained by substituting Eq S13 into Eq S19.

3. Force plots with ruptures at a single tether length

Polymer stretching events that are followed by the abrupt rupture at the tip-sample separation that is noticeably less than the twice single tether length were also detected in the measurements. These events were filtered out before the statistical analysis of rupture forces was performed. For comparison, typical force plots with ruptures at tip-sample separation corresponding to the single and double tether lengths are shown in Figure S2.

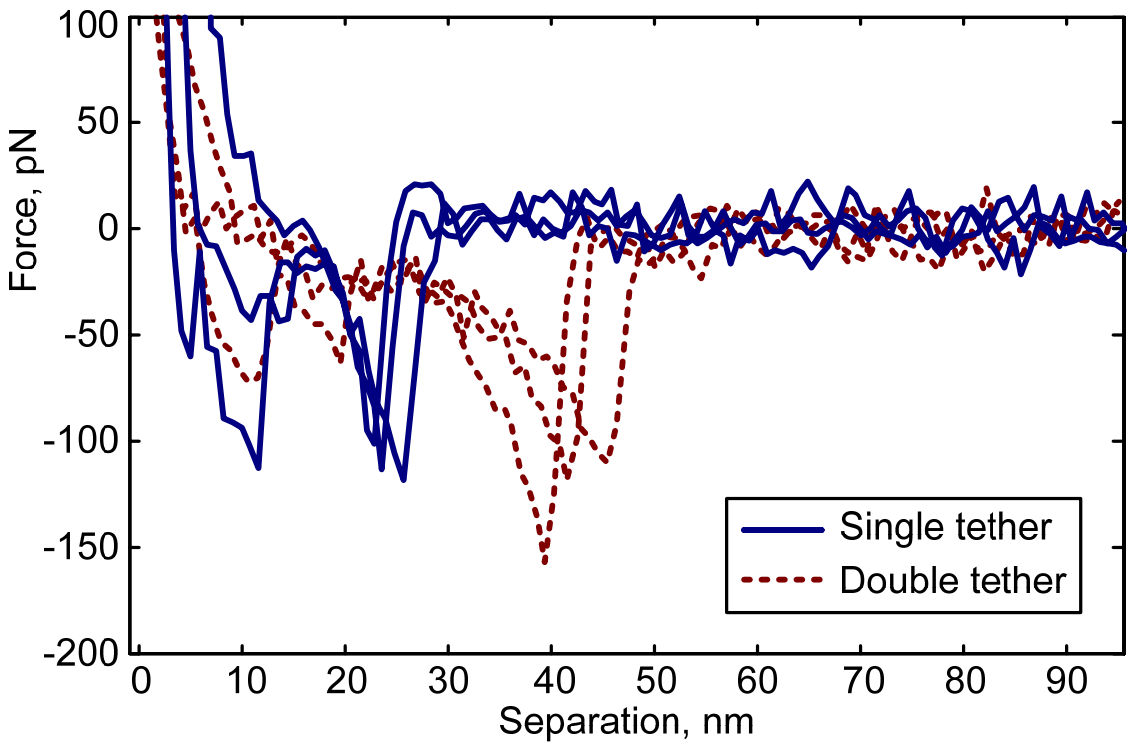

Figure S2. Force plots collected using C60-modified tip and C-60 modified surface. Force plots exhibit variation in the tip-sample separation of the rupture events. Ruptures at the distance less than the length of one polymeric tether are labeled as "Single tether" and ruptures at distances noticeably higher than the length of single tether are labeled as "Double tether"

4. Statistics of the empty tether control experiments

In control experiments both surfaces were grafted with polymeric tethers but fullerenes were attached only to one surface and polymeric linkers on another surface remained "empty". These experiments were testing whether interactions other than fullerene-fullerene interactions could be detected. Few force plots with rupture forces away from the surface were detected in these control experiments. These force plots were analyzed using the same approach as normal force plots; tether contour lengths an rupture forces were extracted. The detection probability of events with the tether contour length in the range for double tether experiment was 0.078%; this detection rate is at least five times lower than the lowest detection probability in "normal" experiments. This supports the assigning the rupture events measured in normal experiments to interactions between tethered fullerene molecules.

Figure S3 shows histograms of rupture forces (panel A) and tether contour lengths (panel B) measured in normal and control experiments. The legends are shown in each graph. The contour lengths are at the lower range of the normal contour lengths; therefore, it might be suggested that the rupture events in control experiments come from C60-surface interactions where tethers have high contour lengths because of tether polydispersity. These interactions also exhibit high rupture force. This also indicates that these interactions are different from the normal C60-C60 ruptures.

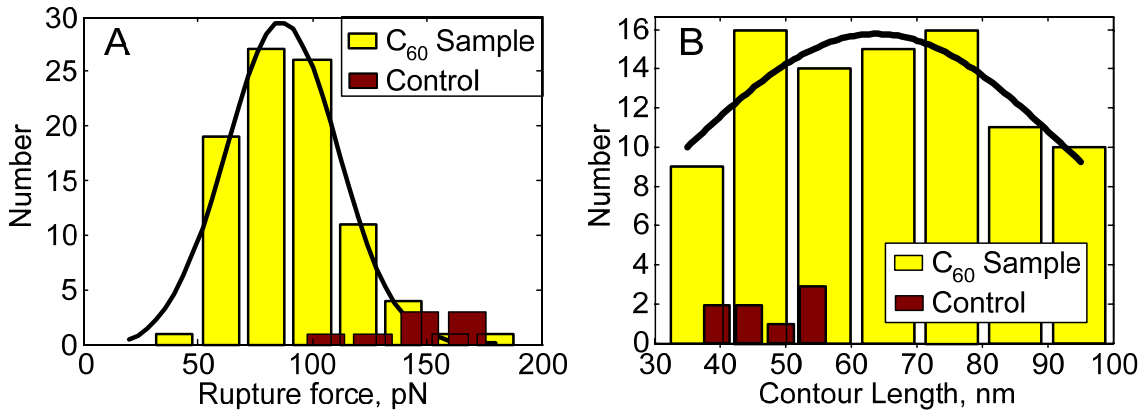

Figure S3. Control experiments with "empty tether". Histograms compare normal and control experiments. Panel A shows distributions of rupture forces and panel B shows distributions of tether lengths. Measurements were performed with 5 µm/s probe velocity.

5. Most probable forces and loading rates

The most probable forces and most probable loading rates were determined as the position of the peak of the Gaussian that fits the data. The Gaussians were multiplied by the window function to account for the limited force sensitivity. Figures S4 and S5 show all histograms of rupture forces and loading rates, respectively. Graphs also include the fit lines that were used to determine the most probable values. Each column corresponds to the data collected with different samples. Each row contains experiments performed at the same probe velocity.

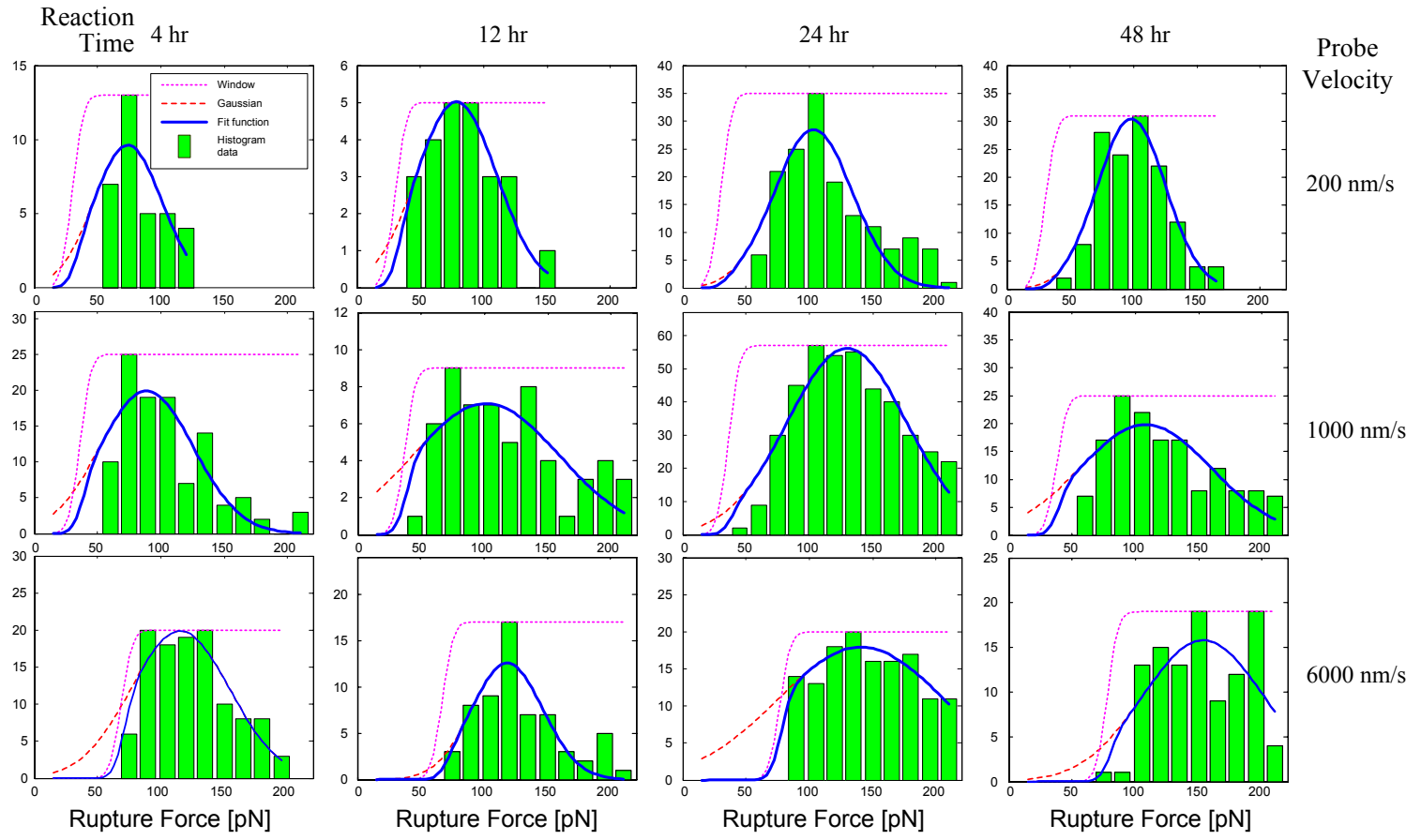

Figure S4. Histograms of the rupture forces and the Gaussian fits to the data

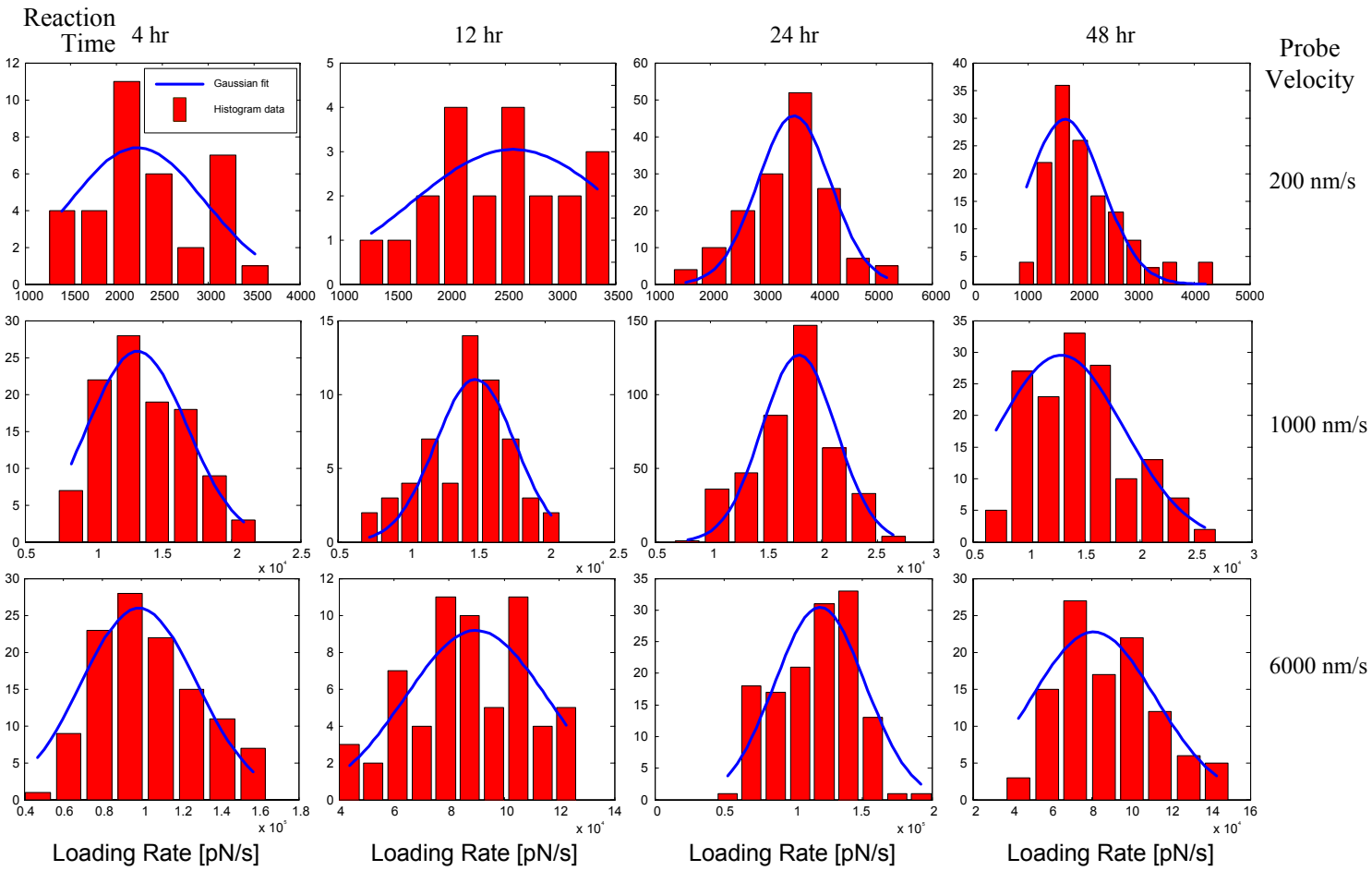

Figure S5. Histograms of the apparent loading rates and the Gaussian fits to the data

References

(1) Ray, C.; Brown, J. R.; Akhremitchev, B. B. *J. Phys. Chem. B* **2007**, *11*, 1963.

(2) Oesterhelt, F.; Rief, M.; Gaub, H. E. *New J. Phys.* **1999**, *1*, 6.1.